

Covalent Organic Frameworks for Carbon Dioxide Capture from Air

Hao Lyu, Haozhe Li, Nikita Hanikel, Kaiyu Wang, and Omar M. Yaghi*

Cite This: *J. Am. Chem. Soc.* 2022, 144, 12989–12995

Read Online

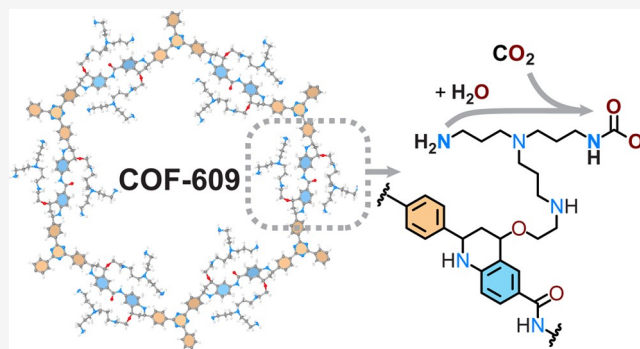
ACCESS |

Metrics & More

Article Recommendations

Supporting Information

ABSTRACT: We report the first covalent incorporation of reactive aliphatic amine species into covalent organic frameworks (COFs). This was achieved through the crystallization of an imine-linked COF, termed COF-609-Im, followed by conversion of its imine linkage to base-stable tetrahydroquinoline linkage through aza-Diels–Alder cycloaddition, and finally, the covalent incorporation of tris(3-aminopropyl)amine into the framework. The obtained COF-609 exhibits a 1360-fold increase in CO₂ uptake capacity compared to the pristine framework and a further 29% enhancement in the presence of humidity. We confirmed the chemistry of framework conversion and corroborated the enhanced CO₂ uptake phenomenon with and without humidity through isotope-labeled Fourier transform infrared spectroscopy and solid-state nuclear magnetic resonance spectroscopy. With this study, we established a new synthetic strategy to access a class of chemisorbents characterized by high affinity to CO₂ in dilute sources, such as the air.



INTRODUCTION

Direct air capture (DAC) of carbon dioxide is an imperative component of the efforts to limit global warming.^{1–4} Capturing CO₂ from air is an interesting chemical problem because it requires the selective removal of CO₂ from a mixture containing other species. The fact that the CO₂ concentration in ambient air is low (0.04%) further compounds the challenge.^{5,6} To capture CO₂ from such a dilute source requires a material with reactive CO₂-specific sites. In this regard, amines are appealing and aqueous solutions of monoethanolamine have already been deployed for such separation.⁷ However, their use requires a large consumption of energy and suffers from operational problems such as decomposition and toxicity. Many classes of solid-state materials have therefore been evaluated for this application to reduce the energy consumption compared to aqueous amine solutions.^{8–22} Here, we report the use of porous covalent organic frameworks (COFs) as solid-state platforms onto which amines could be covalently bound and used for CO₂ capture from air. The use of COFs offers advantages for precision design of framework and modification of the chemical environment within their pores.^{23–26} We show that when such a COF is functionalized with amines, it can capture CO₂ from dry air with a 1360-fold increase in uptake capacity compared to the pristine framework and a further 29% increase in the presence of humidity.

RESULTS AND DISCUSSION

Our COF, termed COF-609, was made by the crystallization of an imine-linked COF backbone, followed by postsynthetic

linkage conversion and amine installation (Figure 1a,b). Specifically, a porous, crystalline, imine-linked COF was first synthesized through imine condensation between 2,4,6-tris(4-formylphenyl)-1,3,5-triazine (TFPT) and 4,4'-diaminobenzanilide (DABA) to give COF-609-Im with the reticular formula [(TFPT)₂(DABA)₃]_{imine}. The crystallization was carried out in a solvent mixture of mesitylene and *n*-butanol, catalyzed by an aqueous solution of acetic acid (see details in Section S2.2). In the second step, COF-609-Im was subsequently used as a reactant, where its imine linkages were converted to tetrahydroquinoline (THQ) linkages by reacting with 2-chloroethyl vinyl ether (CVE) through aza-Diels–Alder cycloaddition catalyzed by Fe³⁺ in diethyl ether (Section S2.3) to form [(TFPT)₂(DABA)₃]_{THQ}.^{27–29} This reaction allowed the COF to withstand strongly basic conditions due to the significantly increased chemical stability compared to its imine-linked precursor. The –Cl group introduced in this step allowed for the installation of tris(3-aminopropyl)amine (TRPN) onto the framework backbone through a nucleophilic substitution reaction, followed by washing with a concentrated potassium hydroxide (KOH) solution to yield COF-609 [(TFPT)₂(DABA)₃(-TRPN)_x]_{THQ} (Section S2.3).

Received: May 20, 2022

Published: July 5, 2022



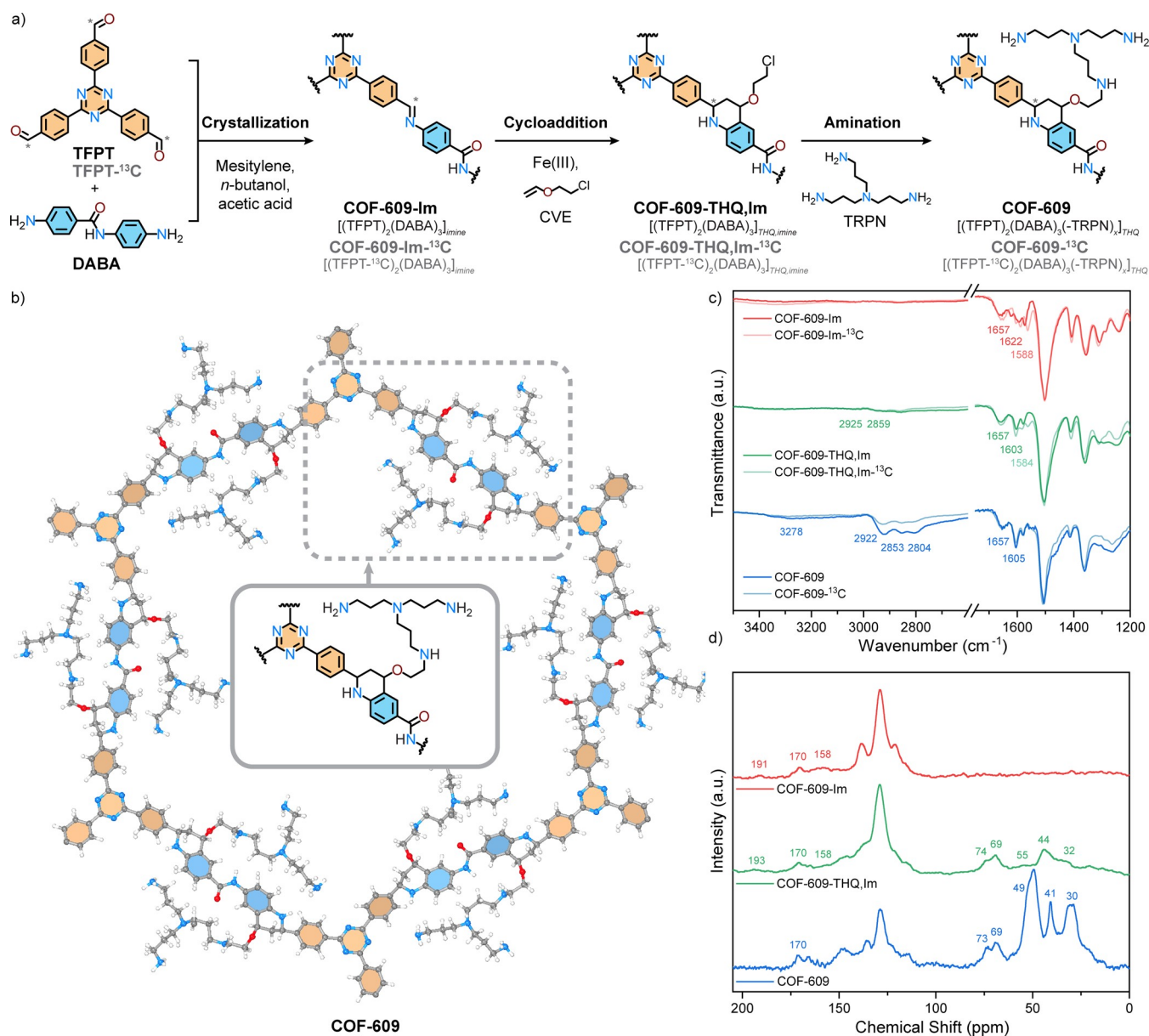


Figure 1. (a) Synthetic scheme of natural abundance and carbonyl- ^{13}C -labeled (gray “*”) COF-609; (b) atomic structure of COF-609; (c) stacked FT-IR spectra of COF-609-Im, COF-609-Im- ^{13}C , COF-609-THQ,Im, COF-609-THQ,Im- ^{13}C , COF-609, and COF-609- ^{13}C ; and (d) stacked CP/MAS solid-state ^{13}C NMR spectra of COF-609-Im, COF-609-THQ,Im, and COF-609. Color code in panel (a): C, gray; H, white; N, blue; and O, red. Aromatic rings are colored to assist the differentiation of the origin of the different moieties.

To monitor this chemistry, we first probed each stage of the synthesis using Fourier transform infrared (FT-IR) spectroscopy. Upon crystallization, the FT-IR spectrum of COF-609-Im was first compared to the spectra of the starting materials, TFPT and DABA (Figure S9). The vibrational absorbance bands at 1694 cm^{-1} (aldehyde $\nu_{\text{C}=\text{O}}$ stretch) and 2819 and 2729 cm^{-1} (aldehyde $\nu_{\text{C}-\text{H}}$ stretches) observed in TFPT were largely diminished in the spectrum of COF-609-Im. Similarly, the absorbance bands at 3394 and 3308 cm^{-1} (amine $\nu_{\text{N}-\text{H}}$ stretches) in DABA were found to be absent in the spectrum of COF-609-Im, whereas the amide $\nu_{\text{C}=\text{O}}$ stretch that was likely overlapping with the strong absorbance of the $\nu_{\text{N}-\text{H}}$ bend at 1624 cm^{-1} in DABA appeared at 1657 cm^{-1} in COF-609-Im. This signified the conversion of the aldehyde and amine functionalities in the starting materials, which was further

corroborated by the observation of the emerging imine $\nu_{\text{C}=\text{N}}$ stretch absorbance at 1622 cm^{-1} in COF-609-Im.

To further confirm the formation of imines, we synthesized carbonyl- ^{13}C -labeled TFPT, termed TFPT- ^{13}C (Section S2.1), and reacted it with DABA following the same procedure to crystallize COF-609-Im- ^{13}C , where the imine linkage was labeled with ^{13}C (Figure 1a). As a result of the isotopic effect, the relevant vibrational absorbance bands exhibited red shifts (Section S3).³⁰ For example, the $\nu_{\text{C}=\text{O}}$ stretch shifted from 1694 cm^{-1} in TFPT to 1654 cm^{-1} in TFPT- ^{13}C , and the $\nu_{\text{C}=\text{N}}$ stretch shifted from 1622 cm^{-1} in COF-609-Im to 1588 cm^{-1} in COF-609-Im- ^{13}C , both in good agreement with calculated shifts using a simple harmonic oscillator model (Table S1). The absorbance signals attributed to the unlabeled parts of the framework were coincident, while those of the linkage were shifted (Figure 1b).

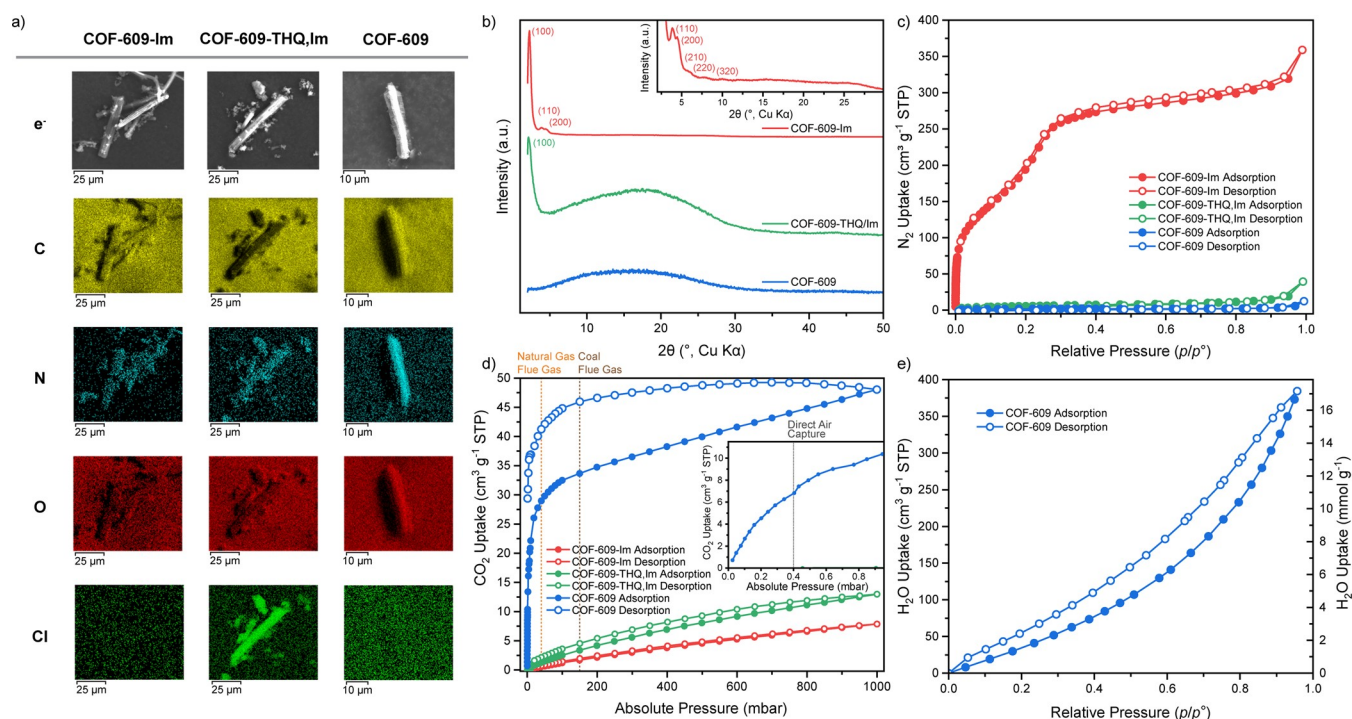


Figure 2. (a) Scanning electron micrographs and elemental maps, (b) PXRD patterns, (c) N_2 sorption isotherms (77 K), and (d) single-component CO_2 isotherms (25 °C) of COF-609-Im, COF-609-THQ,Im, and COF-609, as well as (e) single-component H_2O isotherm of COF-609 at 25 °C. The inset in panel (b) provides a zoomed-in view of the PXRD pattern of COF-609-Im, highlighting low-intensity reflections. The inset in panel (d) displays a zoomed-in view of the adsorption branch of COF-609 at 0–1 mbar to highlight the uptake at the DAC-relevant pressure.

In the following step, the absorbance at 1622 cm^{-1} (imine $\nu_{C=N}$ stretch) in COF-609-THQ,Im was largely diminished and possibly merged with the absorbance at 1603 cm^{-1} . This was confirmed by the presence of the signal at 1584 cm^{-1} in COF-609-THQ,Im- ^{13}C (Figures 1c and S10). This observation indicated the coexistence of THQ and imine linkages in the product of the aza-Diels–Alder cycloaddition reaction. The emergence of broad absorbance bands at 2925 and 2859 cm^{-1} in both samples indicated the introduction of aliphatic C–H bonds as part of the THQ linkage and the 2-chloroethoxyl side chain. In the last step, the higher intensity of the absorbance bands at 2922 , 2853 , and 2804 cm^{-1} indicated the introduction of aliphatic amines through nucleophilic substitution, which also contributed to the broad absorbance band at 3278 cm^{-1} (ν_{N-H} stretch, Figures 1c and S10). Throughout the process, the absorbance at 1657 cm^{-1} (amide $\nu_{C=O}$ stretch) remained unchanged, indicating that the amide introduced in DABA remained intact during the postsynthetic modification.

Solid-state nuclear magnetic resonance (ssNMR) spectroscopy measurements on the COF samples further evidenced the two-step postsynthetic transformation. Cross-polarization magic-angle spinning (CP-MAS) ^{13}C ssNMR spectra were collected on unlabeled COF-609-Im, COF-609-THQ,Im, and COF-609 samples (Figure 1d), where the signal at 158 ppm (assigned to the imine C) in COF-609-Im was found attenuated in COF-609-THQ,Im and further diminished in COF-609. By contrast, the signals at 62–81 ppm (assigned to the α -C of the ether O) and at 27–49 ppm (assigned to aliphatic C atoms in the THQ linkage and ether side chain) were found in COF-609-THQ,Im while being absent in COF-609-Im. In the second transformation step, the signals at 62–81 ppm (the α -C of the ether O) were mostly unaltered in the

aminated product COF-609, while the newly emerged signals at 44–59 ppm (assigned to the α -C of the amine N) and at 11–44 ppm (assigned to other aliphatic C atoms in the THQ linkages and amine side chains) signified the covalent installation of the aliphatic amine, TRPN, onto the side chains of COF-609-THQ,Im. Throughout these modifications, the other motifs in the COF backbone, such as aromatic rings (109–151 ppm), triazine, and amide (163–178 ppm), were found to be mostly unaltered.

Energy-dispersive X-ray spectroscopy (EDS) mapping of the COF samples using a scanning electron microscope (SEM, Figure 2a) revealed that Cl elements were absent in COF-609-Im, homogeneously distributed among crystallites of COF-609-THQ,Im, and finally absent in COF-609. Collectively, the evidence above indicated that, after crystallization of COF-609-Im, the aza-Diels–Alder cycloaddition largely converted the imine linkages to form THQ linkages. These withstood the nucleophilic amination reaction and provided the sites (–Cl groups) onto which the aliphatic amines were covalently installed—all in good agreement with the proposed scheme of transformation. Thermogravimetric analysis (TGA) on the three stages of synthesis revealed that a different profile started to appear at the second step, where the thermal degradation of the THQ linkages induced a weight loss at $\sim 200\text{ °C}$ for both COF-609-THQ,Im and COF-609 (Section S5). This provided further evidence of the transformation.

The ^{13}C labeling of the linkage in COF-609 allowed for the quantitative study of this chemistry due to the significantly enhanced signal of the ^{13}C -labeled carbon in contrast to the unlabeled carbon signals on the rest of the framework. Multiple contact periods magic-angle spinning (MultiCP/MAS) solid-state NMR experiments provided a powerful tool to estimate

the ratio of the labeled species in the COF samples by comparing the integration of the signals assigned to each species.³¹ The COF-609-Im-¹³C sample was found to contain 94% ¹³C-labeled imine linkages at 158 ppm, while a 6% residual ¹³C-labeled aldehyde signal was found at 191 ppm, which was attributed to defect sites in the framework. COF-609-THQ₂Im-¹³C was found to comprise 40% THQ (56 ppm), 54% imine (159 ppm), and 6% aldehyde (194 ppm) that was unaltered during the cycloaddition. The amination step eliminated the residual aldehyde signals, likely attributed to decomposition of such defect sites. The imine (157 ppm) composition decreased to 42%, whereas THQ (~55 ppm) increased to 58%. These changes were attributed to the partial decomposition of the remaining imine linkages of COF-609-THQ₂Im in the amine solution (Figure S18). This measurement also helped to further confirm the speciation based on CP/MAS ssNMR measurements. The signal of the ¹³C-labeled THQ carbon displays a broad profile with shoulder peaks at ~50 and ~66 ppm, indicating the presence of a distribution of isomers as a result of the aza-Diels–Alder cycloaddition.

Combined analyses using SEM, powder X-ray diffraction (PXRD), and N₂ sorption isotherms were conducted on the COF-609 series to elucidate their structures and monitor the changes throughout the transformation. COF-609-Im crystallized into needle-shaped fibrous aggregates (Figure 2a). This morphology remained mostly unaltered before and after cycloaddition and amination reactions, despite the changes in terms of elemental compositions and functionalities.

PXRD patterns of activated COF-609-Im displayed strong Bragg diffraction signals at 2.2, 3.9, and 4.5° and broad reflections distinguishable at 6.0, 7.8, and 9.9° (Figure 2b). These are in good agreement with a structural model in which TFPT and DABA are linked through imine bonds to form honeycomb sheets stacked in an eclipsed fashion. Such structures form one-dimensional channel-shaped pores along the stacking direction. These were studied through N₂ sorption isotherm measurements performed on COF-609-Im at 77 K (Figure 2c) to reveal that the pores of COF-609-Im were accessible to N₂, with a Brunauer–Emmett–Teller (BET) surface area of 724 m² g⁻¹ (Figure S16). Fitting of the isotherm based on nonlocal density functional theory indicated a uniform pore size distribution featuring a narrow peak at 37 Å diameter (Figure S17). This is in good agreement with the eclipsed stacking model, where the wall-to-wall distance of the van der Waals surface of the channel is estimated to be 39 Å. The model was subjected to Pawley refinement against the PXRD pattern to yield a unit cell in space group P3, with unit cell parameters *a* = 45.7 Å and *c* = 3.5 Å (Figure S11). PXRD patterns of the cycloaddition product COF-609-THQ₂Im indicated a significant decrease in crystallinity, where only the major reflection at 2.2° was observed (Figure 2b). This can be attributed to the nonplanarity of the THQ linkages and the possible presence of stereoisomers as was indicated above. A geometrically optimized atomic model of COF-609-THQ was generated based on the model of COF-609-Im assuming 100% conversion to THQ linkages, of which the prediction of the PXRD pattern exhibited good agreement with the experimental pattern (Figure S12). However, it is noteworthy that the presence of residual imine-linked regions can also contribute to this diffraction.

N₂ isotherm measurement of COF-609-THQ₂Im indicated that the interior of the framework was no longer accessible to N₂ at the measurement conditions, which can be attributed to

the disorder introduced by the conversion (Figure 2c). However, substitution of the –Cl group by amines in the amination step indicated that it was still accessible to TRPN and consequently allowed for the installation of amines. PXRD patterns of the resulting COF-609 exhibited mostly amorphous features (Figure 2b), and N₂ sorption isotherm analysis indicated limited porosity (Figure 2c) similar to that of COF-609-THQ₂Im. This was attributed to the existing disorder of the framework and, moreover, the flexible nature of the large population of aliphatic amines introduced into the pore channels. Nevertheless, since the framework connectivity remains unaltered even with amine installation, the resulting material is suitable for CO₂ capture.

To probe this, single-component CO₂ sorption isotherms of COF-609-Im, COF-609-THQ₂Im, and COF-609 were measured at 25 °C and compared as shown in Figure 2d. COF-609-Im, despite being the most porous, exhibited the lowest CO₂ uptake in the entire range of experiment (0–1000 mbar). The lack of a sharp increase in the low-pressure region and a minimal hysteresis indicated that the framework had a low affinity to CO₂ and physisorption-dominant characteristics. COF-609-THQ₂Im exhibited a slight increase in CO₂ uptake compared to its precursor and a more significant hysteresis indicating weak chemisorption. This was attributed to the increased polarity and the introduction of a secondary amine (–NH–) in the THQ linkage resulting from the cycloaddition reaction. By contrast, the CO₂ sorption isotherm of COF-609 displayed a steep rise in the adsorption branch at very low CO₂ pressures, turning into a moderate slope between 50 and 1000 mbar, and a hysteresis between the adsorption and desorption branches. Both of these observations indicated strong chemisorption interactions that cannot be readily reversed using only vacuum. Although examples of the introduction of amine,³² hydroxyl,³³ and epoxide³⁴ species have been reported in COFs, this is the first example of strong chemisorption of CO₂ in COFs.

Specifically, COF-609 adsorbs 6.8 cm³ g⁻¹ STP (0.304 mmol g⁻¹) at 0.4 mbar CO₂ (conditions relevant to DAC), a 1360-fold increase compared to that of COF-609-THQ₂Im, which adsorbs 0.005 cm³ g⁻¹ STP (0.00022 mmol g⁻¹) at 0.4 mbar CO₂ pressure (COF-609-Im's isotherm was out of range at this pressure due to very low uptake). At 40 mbar (relevant to postcombustion capture from natural gas flue gas), COF-609 adsorbs 29.0 cm³ g⁻¹ STP (1.29 mmol g⁻¹) CO₂, a 53-fold increase from COF-609-Im (0.54 cm³ g⁻¹ STP, 0.024 mmol g⁻¹) or 23-fold from COF-609-THQ₂Im (1.27 cm³ g⁻¹ STP, 0.057 mmol g⁻¹). At 150 mbar (relevant to postcombustion capture from coal flue gas), the CO₂ uptake of COF-609 (33.7 cm³ g⁻¹ STP, 1.50 mmol g⁻¹) is 20-fold higher than that of COF-609-Im (1.70 cm³ g⁻¹ STP, 0.076 mmol g⁻¹) or 10-fold higher than that of COF-609-THQ₂Im (3.40 cm³ g⁻¹ STP, 0.151 mmol g⁻¹).

The significant increase of CO₂ uptake provided strong evidence that the introduction of strong chemisorption through incorporating aliphatic amines into COFs points to great potential for such sorbents for efficient DAC and postcombustion capture. As most capturing scenarios involve a feed containing water, it is of vital importance to examine the CO₂ uptake performance of COF-609 in the presence of humidity. We thus tested COF-609 in a dynamic breakthrough system (Section S8), where an activated sample was first saturated in a mixture of 79% N₂ and 21% O₂ with a relative humidity (RH) of 50% at 25 °C and 1 atm and was then

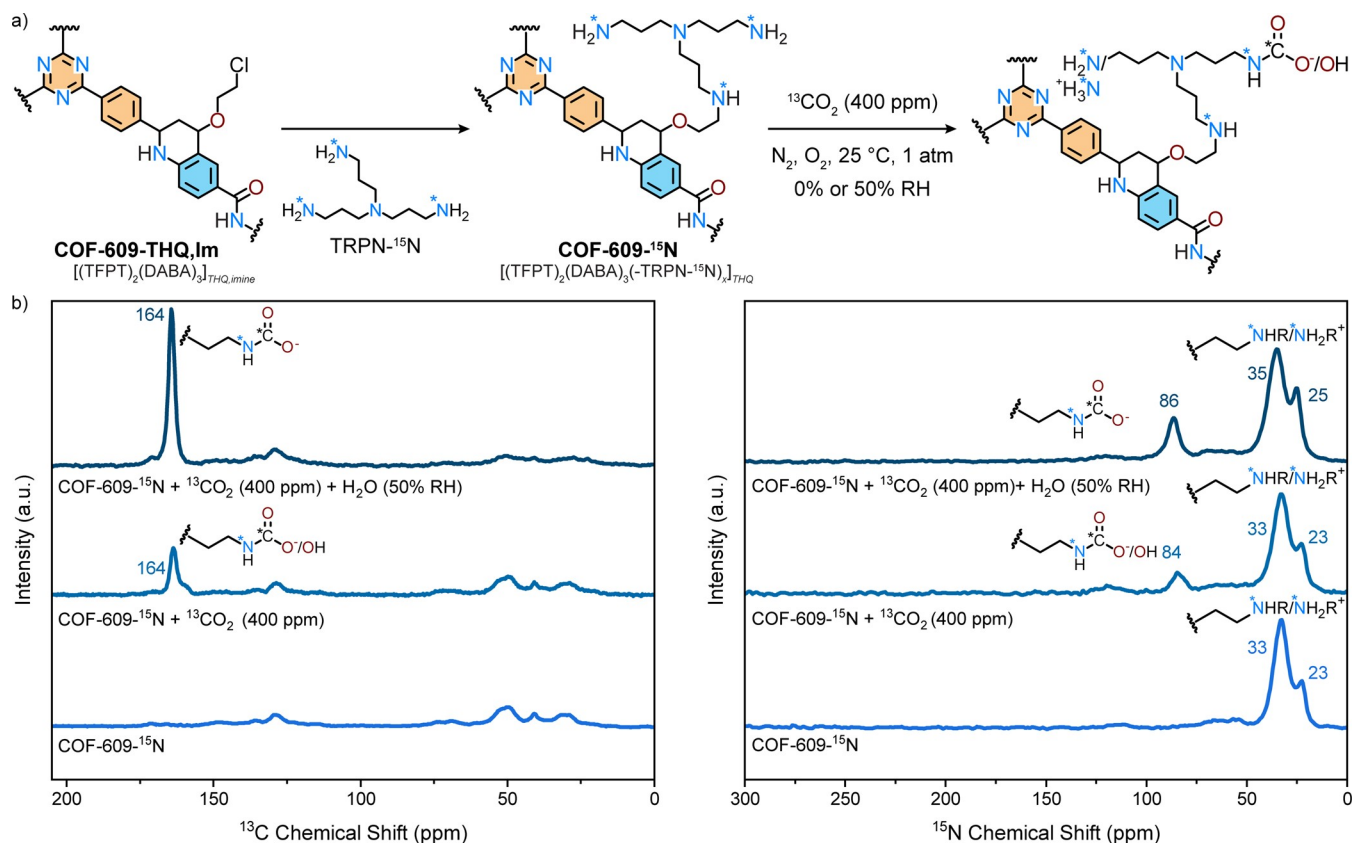


Figure 3. (a) Schematics of the synthesis of COF-609-¹⁵N and its chemisorption of ¹³CO₂ and (b) ¹³C and ¹⁵N solid-state NMR spectra of ¹³CO₂ dosing experiments performed on COF-609-¹⁵N (bottom) under dry (middle) and humid (top) conditions. Illustrative schemes of major sorption products are provided to highlight the assignments of signals and chemical conversion of species. Isotopic labeling sites are marked with "*" for ¹³C (black) and ¹⁵N (30%, blue). R = H for primary amine groups or aliphatic chains for secondary amine groups.

exposed to a mixture of 0.04% (400 ppm) CO₂, 79% N₂, and 21% O₂ with an RH of 50% at 25 °C and 1 atm. Numerical integration of the monitored concentrations revealed that the CO₂ uptake of COF-609 from 400 ppm CO₂ in the presence of 50% RH at 25 °C and 1 atm was 0.393 mmol g⁻¹, a 29% enhancement compared to its single-component dry CO₂ uptake.

Additionally, the H₂O vapor sorption isotherm of COF-609 measured at 25 °C (Figure 2e) yielded that the H₂O uptake of COF-609 at 50% RH and 25 °C was 104.3 cm³ g⁻¹ STP (4.66 mmol g⁻¹), a relatively low value compared to more polar chemisorbents, such as MOF-808-Gly.³⁵ This has the beneficial effect that a significant amount of energy consumption due to water desorption in heat-driven cycling can be reduced in this class of chemisorbents, as is exemplified by COF-609. However, the amount of water taken up was enough to enhance the CO₂ uptake compared to the dry state, as is evidenced by the dynamic breakthrough results above.

In the final step, we studied the chemistry of CO₂ capture with the reactive amine species in COF-609, both in the dry state and in the presence of moisture (Figure 3a,b). We first synthesized terminal amine-¹⁵N-labeled TRPN (TRPN-¹⁵N, Section S2.1), which reacted with COF-609-THQ,Im to form 30% ¹⁵N-labeled COF-609, termed COF-609-¹⁵N (Figure 3a). The CP/MAS solid-state ¹³C NMR spectrum of COF-609-¹⁵N largely resembled that of unlabeled COF-609. Its ¹⁵N spectrum was characterized by two predominant peaks at 23 and 33 ppm, which were attributed to ¹⁵N-labeled primary and secondary amines on the side chains of COF-609-¹⁵N. Upon

exposing COF-609-¹⁵N to a stream of gas composed of 0.04% ¹³CO₂, 79% N₂, and 21% O₂ with 0% RH at 25 °C and 1 atm, a major signal at 164 ppm emerged in the ¹³C spectrum. This was accompanied by the emergence of a new signal at 84 ppm in the ¹⁵N spectrum, indicating the formation of carbamate species. Presaturation of COF-609-¹⁵N at 50% RH in 79% N₂ and 21% O₂ at 25 °C followed by exposure to the same gas stream but with additional 0.04% ¹³CO₂ led to a significantly intensified signal at 164 ppm in the ¹³C spectrum and a similar rise of the signal at 86 ppm in the ¹⁵N spectrum. This result indicates that the major product of chemisorption of low-concentration CO₂ in COF-609 is carbamate, where the presence of water considerably boosts its formation, resulting in an enhanced uptake in the presence of moisture.^{35,36} The retention of the amine ¹⁵N signals at 23 and 33 ppm for COF-609-¹⁵N in dry ¹³CO₂ (400 ppm) as well as 25 and 35 ppm for COF-609-¹⁵N in humid ¹³CO₂ (400 ppm, RH 50%) indicated the presence of excess amines and their likely role of facilitating carbamic acid deprotonation to form stronger-binding carbamates in humid conditions, which helped increase the uptake capacity of CO₂. This is in good agreement with the single-component CO₂ isotherm and the dynamic CO₂/H₂O breakthrough measurements.

CONCLUSIONS

Our approach in stabilizing and covalently installing aliphatic amines into COFs using judicious choices of organic reactions has proved effective in incorporating the CO₂-carbamate chemistry into stable porous adsorbents. This leads to efficient

CO₂ uptake capability from very diluted sources and in the presence of water, such as capturing CO₂ directly from air.

■ ASSOCIATED CONTENT

SI Supporting Information

The Supporting Information is available free of charge at <https://pubs.acs.org/doi/10.1021/jacs.2c05382>.

Detailed experimental procedures and data for reported compounds, supplementary figures and tables for characterization, and description of instrumental setups (PDF)

■ AUTHOR INFORMATION

Corresponding Author

Omar M. Yaghi – Department of Chemistry and Kavli Energy Nanoscience Institute, University of California, Berkeley, Berkeley, California 94720, United States; KACST-UC Berkeley Center of Excellence for Nanomaterials for Clean Energy Applications, King Abdulaziz City for Science and Technology, Riyadh 11442, Saudi Arabia; orcid.org/0000-0002-5611-3325; Email: yaghi@berkeley.edu

Authors

Hao Lyu – Department of Chemistry and Kavli Energy Nanoscience Institute, University of California, Berkeley, Berkeley, California 94720, United States; orcid.org/0000-0001-7393-2456

Haozhe Li – Department of Chemistry and Kavli Energy Nanoscience Institute, University of California, Berkeley, Berkeley, California 94720, United States

Nikita Hanikel – Department of Chemistry and Kavli Energy Nanoscience Institute, University of California, Berkeley, Berkeley, California 94720, United States; orcid.org/0000-0002-3292-5070

Kaiyu Wang – Department of Chemistry and Kavli Energy Nanoscience Institute, University of California, Berkeley, Berkeley, California 94720, United States

Complete contact information is available at:

<https://pubs.acs.org/doi/10.1021/jacs.2c05382>

Author Contributions

The manuscript was written through contributions of all authors. All authors have given approval to the final version of the manuscript.

Funding

The synthesis and CO₂ uptake isotherm measurements of COF-609 compounds were supported by the Department of Energy under Award Number DE-FE0031956.

Notes

The authors declare the following competing financial interest(s): This work has been filed as US Provisional Patent Application No. 63/329,369.

The solid-state NMR data in this work are also available at <https://doi.org/10.6078/D1F412>.

This report was prepared as an account of work sponsored by an agency of the United States Government. Neither the United States Government nor any agency thereof, nor any of their employees, makes any warranty, express or implied, or assumes any legal liability or responsibility for the accuracy, completeness, or usefulness of any information, apparatus, product, or process disclosed, or represents that its use would not infringe privately owned rights. Reference herein to any

specific commercial product, process, or service by trade name, trademark, manufacturer, or otherwise does not necessarily constitute or imply its endorsement, recommendation, or favoring by the United States Government or any agency thereof. The views and opinions of authors expressed herein do not necessarily state or reflect those of the United States Government or any agency thereof.

This work has been filed as US Provisional Patent Application No. 63/329,369.

■ ACKNOWLEDGMENTS

The authors thank Dr. Alicia Lund for her support with solid-state NMR instrumentation and measurements, and Dr. Tianqiong Ma for her help with SEM measurements. The authors thank Oscar Iu-Fan Chen, Zihui Zhou, Dr. Daria Kurandina, Dr. Wentao Xu, Dr. David R. Moore, Dr. Mark D. Doherty, and Prof. T. Grant Glover for helpful discussions. N.H. thanks for support through a Kavli ENSI Philomathia Graduate Student Fellowship and a Blavatnik Innovation Fellowship. The NMR facility in the College of Chemistry at UC Berkeley is supported in part by NIH S10OD024998. The instrument used in part of the solid-state NMR measurements is supported by the National Science Foundation under Grant No. 2018784.

■ REFERENCES

- (1) *Negative Emissions Technologies and Reliable Sequestration: A Research Agenda*; The National Academies Press: Washington, DC, 2019. DOI: 10.17226/25259.
- (2) Climate Change 2022: Mitigation of Climate Change. <https://www.ipcc.ch/report/ar6/wg3/> (accessed May 03, 2022).
- (3) Bui, M.; Adjiman, C. S.; Bardow, A.; Anthony, E. J.; Boston, A.; Brown, S.; Fennell, P. S.; Fuss, S.; Galindo, A.; Hackett, L. A.; Hallett, J. P.; Herzog, H. J.; Jackson, G.; Kemper, J.; Krevor, S.; Maitland, G. C.; Matuszewski, M.; Metcalfe, I. S.; Petit, C.; Puxty, G.; Reimer, J.; Reiner, D. M.; Rubin, E. S.; Scott, S. A.; Shah, N.; Smit, B.; Trusler, J. P. M.; Webley, P.; Wilcox, J.; Mac Dowell, N. Carbon Capture and Storage (CCS): The Way Forward. *Energy Environ. Sci.* **2018**, *11*, 1062–1176.
- (4) *Accelerating Decarbonization of the U.S. Energy System*; The National Academies Press: Washington, DC, 2021. DOI: 10.17226/25932.
- (5) Sanz-Pérez, E. S.; Murdock, C. R.; Didas, S. A.; Jones, C. W. Direct Capture of CO₂ from Ambient Air. *Chem. Rev.* **2016**, *116*, 11840–11876.
- (6) McQueen, N.; Gomes, K. V.; McCormick, C.; Blumanthal, K.; Pisciotta, M.; Wilcox, J. A Review of Direct Air Capture (DAC): Scaling up Commercial Technologies and Innovating for the Future. *Prog. Energy* **2021**, *3*, No. 032001.
- (7) Kiani, A.; Jiang, K.; Feron, P. Techno-Economic Assessment for CO₂ Capture from Air Using a Conventional Liquid-Based Absorption Process. *Front. Energy Res.* **2020**, *8*, 92.
- (8) Keith, D. W.; Holmes, G.; St Angelo, D.; Heidel, K. A Process for Capturing CO₂ from the Atmosphere. *Joule* **2018**, *2*, 1573–1594.
- (9) Stuckert, N. R.; Yang, R. T. CO₂ Capture from the Atmosphere and Simultaneous Concentration Using Zeolites and Amine-Grafted SBA-15. *Environ. Sci. Technol.* **2011**, *45*, 10257–10264.
- (10) Nugent, P.; Belmabkhout, Y.; Burd, S. D.; Cairns, A. J.; Luebke, R.; Forrest, K.; Pham, T.; Ma, S.; Space, B.; Wojtas, L.; Eddaoudi, M.; Zaworotko, M. J. Porous Materials with Optimal Adsorption Thermodynamics and Kinetics for CO₂ Separation. *Nature* **2013**, *495*, 80–84.
- (11) Shekhah, O.; Belmabkhout, Y.; Chen, Z.; Guillerm, V.; Cairns, A.; Adil, K.; Eddaoudi, M. Made-to-Order Metal-Organic Frameworks for Trace Carbon Dioxide Removal and Air Capture. *Nat. Commun.* **2014**, *5*, No. 4228.

- (12) Didas, S. A.; Choi, S.; Chaikittisilp, W.; Jones, C. W. Amine–Oxide Hybrid Materials for CO₂ Capture from Ambient Air. *Acc. Chem. Res.* **2015**, *48*, 2680–2687.
- (13) Chaikittisilp, W.; Khunsupat, R.; Chen, T. T.; Jones, C. W. Poly(Allylamine)–Mesoporous Silica Composite Materials for CO₂ Capture from Simulated Flue Gas or Ambient Air. *Ind. Eng. Chem. Res.* **2011**, *50*, 14203–14210.
- (14) Liao, P.-Q.; Chen, X.-W.; Liu, S.-Y.; Li, X.-Y.; Xu, Y.-T.; Tang, M.; Rui, Z.; Ji, H.; Zhang, J.-P.; Chen, X.-M. Putting an Ultrahigh Concentration of Amine Groups into a Metal–Organic Framework for CO₂ Capture at Low Pressures. *Chem. Sci.* **2016**, *7*, 6528–6533.
- (15) Belmabkhout, Y.; Serna-Guerrero, R.; Sayari, A. Amine-Bearing Mesoporous Silica for CO₂ Removal from Dry and Humid Air. *Chem. Eng. Sci.* **2010**, *65*, 3695–3698.
- (16) Sayari, A.; Liu, Q.; Mishra, P. Enhanced Adsorption Efficiency through Materials Design for Direct Air Capture over Supported Polyethylenimine. *ChemSusChem* **2016**, *9*, 2796–2803.
- (17) Gebald, C.; Wurzbacher, J. A.; Tingaut, P.; Zimmermann, T.; Steinfeld, A. Amine-Based Nanofibrillated Cellulose as Adsorbent for CO₂ Capture from Air. *Environ. Sci. Technol.* **2011**, *45*, 9101–9108.
- (18) Gebald, C.; Wurzbacher, J. A.; Borgschulte, A.; Zimmermann, T.; Steinfeld, A. Single-Component and Binary CO₂ and H₂O Adsorption of Amine-Functionalized Cellulose. *Environ. Sci. Technol.* **2014**, *48*, 2497–2504.
- (19) Choi, S.; Watanabe, T.; Bae, T.-H.; Sholl, D. S.; Jones, C. W. Modification of the Mg/DOBDC MOF with Amines to Enhance CO₂ Adsorption from Ultradilute Gases. *J. Phys. Chem. Lett.* **2012**, *3*, 1136–1141.
- (20) McDonald, T. M.; Lee, W. R.; Mason, J. A.; Wiers, B. M.; Hong, C. S.; Long, J. R. Capture of Carbon Dioxide from Air and Flue Gas in the Alkylamine-Appended Metal–Organic Framework mmen-Mg₂(dobpdc). *J. Am. Chem. Soc.* **2012**, *134*, 7056–7065.
- (21) Wang, J.; Wang, M.; Li, W.; Qiao, W.; Long, D.; Ling, L. Application of Polyethylenimine-Impregnated Solid Adsorbents for Direct Capture of Low-Concentration CO₂. *AIChE J.* **2015**, *61*, 972–980.
- (22) Kong, Y.; Shen, X.; Cui, S.; Fan, M. Facile Synthesis of an Amine Hybrid Aerogel with High Adsorption Efficiency and Regenerability for Air Capture via a Solvothermal-Assisted Sol–Gel Process and Supercritical Drying. *Green Chem.* **2015**, *17*, 3436–3445.
- (23) Côté, A. P.; Benin, A. I.; Ockwig, N. W.; O’Keeffe, M.; Matzger, A. J.; Yaghi, O. M. Porous, Crystalline, Covalent Organic Frameworks. *Science* **2005**, *310*, 1166–1170.
- (24) Waller, P. J.; Gándara, F.; Yaghi, O. M. Chemistry of Covalent Organic Frameworks. *Acc. Chem. Res.* **2015**, *48*, 3053–3063.
- (25) Diercks, C. S.; Yaghi, O. M. The Atom, the Molecule, and the Covalent Organic Framework. *Science* **2017**, *355*, No. eaal1585.
- (26) Lyle, S. J.; Osborn Popp, T. M.; Waller, P. J.; Pei, X.; Reimer, J. A.; Yaghi, O. M. Multistep Solid-State Organic Synthesis of Carbamate-Linked Covalent Organic Frameworks. *J. Am. Chem. Soc.* **2019**, *141*, 11253–11258.
- (27) Li, C.; Ma, Y.; Liu, H.; Tao, L.; Ren, Y.; Chen, X.; Li, H.; Yang, Q. Asymmetric Photocatalysis over Robust Covalent Organic Frameworks with Tetrahydroquinoline Linkage. *Chin. J. Catal.* **2020**, *41*, 1288–1297.
- (28) Cabral, J.; Laszlo, P.; Montaufer, M. T. Schizoid Reactivity of N-Benzylidene Aniline toward Clay-Catalyzed Cycloadditions. *Tetrahedron Lett.* **1988**, *29*, 547–550.
- (29) Cabral, J.; Laszlo, P. Product Distribution in Diels–Alder Addition of N-Benzylidene Aniline and Enol Ethers. *Tetrahedron Lett.* **1989**, *30*, 7237–7238.
- (30) Lyu, H.; Diercks, C. S.; Zhu, C.; Yaghi, O. M. Porous Crystalline Olefin-Linked Covalent Organic Frameworks. *J. Am. Chem. Soc.* **2019**, *141*, 6848–6852.
- (31) Johnson, R. L.; Schmidt-Rohr, K. Quantitative Solid-State ¹³C NMR with Signal Enhancement by Multiple Cross Polarization. *J. Magn. Reson.* **2014**, *239*, 44–49.
- (32) Guan, X.; Li, H.; Ma, Y.; Xue, M.; Fang, Q.; Yan, Y.; Valtchev, V.; Qiu, S. Chemically Stable Polyarylether-Based Covalent Organic Frameworks. *Nat. Chem.* **2019**, *11*, 587–594.
- (33) Maia, R. A.; Lopes Oliveira, F.; Ritleng, V.; Wang, Q.; Louis, B.; Mothé Esteves, P. CO₂ Capture by Hydroxylated Azine-Based Covalent Organic Frameworks. *Chem. – Eur. J.* **2021**, *27*, 8048–8055.
- (34) Li, Y.; Zhang, J.; Zuo, K.; Li, Z.; Wang, Y.; Hu, H.; Zeng, C.; Xu, H.; Wang, B.; Gao, Y. Covalent Organic Frameworks for Simultaneous CO₂ Capture and Selective Catalytic Transformation. *Catalysts* **2021**, *11*, 1133.
- (35) Lyu, H.; Chen, O. I.-F.; Hanikel, N.; Hossain, M. I.; Flaig, R. W.; Pei, X.; Amin, A.; Doherty, M. D.; Impastato, R. K.; Glover, T. G.; Moore, D. R.; Yaghi, O. M. Carbon Dioxide Capture Chemistry of Amino Acid Functionalized Metal–Organic Frameworks in Humid Flue Gas. *J. Am. Chem. Soc.* **2022**, *144*, 2387–2396.
- (36) Flaig, R. W.; Osborn Popp, T. M.; Fracaroli, A. M.; Kapustin, E. A.; Kalmutzki, M. J.; Altamimi, R. M.; Fathieh, F.; Reimer, J. A.; Yaghi, O. M. The Chemistry of CO₂ Capture in an Amine-Functionalized Metal–Organic Framework under Dry and Humid Conditions. *J. Am. Chem. Soc.* **2017**, *139*, 12125–12128.